Robust Tuning of Cascaded PI Controllers for Three-Phase Vienna Rectifiers Using Multi-Scenario Min-Max Cost

Mohammed Obayes Yousif[a,1,*]

[a] *Al-Furat Al-Awsat Technical University, Al-Musayyib Polytechnic College, Iraq*
[1] *inm.moh2@atu.edu.iq**
*** corresponding author*

ARTICLE INFO

Article history
Received Sep 22, 2026
Received Sep 22, 2026
Revised Oct 28, 2026
Accepted Nov 8, 2026

Keywords
Vienna rectifier
cascaded PI control
genetic algorithm
robust tuning
weak grid
min-max optimization

ABSTRACT

The three-phase Vienna rectifier is widely used for power factor correction in electric-vehicle fast chargers, and its performance depends on the gains of the cascaded PI controllers in the current, DC-link voltage and neutral-point voltage loops. Metaheuristic tuning is usually performed at a single operating point, which may fail when the load, grid strength or component values change. This paper proposes a multi-scenario min-max tuning procedure in which the six PI gains are evaluated over nine training scenarios covering light and rated load, load steps, weak grid, grid unbalance and inductance/capacitance mismatch, and a genetic algorithm (GA) minimises the worst-case cost. The proposed controller is compared with two analytically designed controllers (20 Hz and 50 Hz voltage-loop bandwidth), a single-scenario GA and a particle swarm optimiser (PSO) using the same robust cost. All controllers are evaluated in MATLAB simulation on twelve scenarios, three of which are unseen during tuning, using averaged and PWM-switched models and five random seeds. The single-scenario GA performs best near its training point but reaches a current THD of 21.3% and a power factor of 0.78 in the harshest weak-grid scenario. The robust GA limits the worst-case THD to 2.56%, compared with 4.12% and 4.46% for the manual designs, keeps the power factor at or above 0.9996, and achieves a worst-case DC-link deviation of 4.3 V with an 18.3 ms settling time. Robust GA and PSO give nearly identical results, showing that robustness stems from the min-max formulation rather than from the optimiser.

I. Introduction

The three-phase Vienna rectifier is a three-level boost-type power factor correction (PFC) converter that achieves a high power factor and low line-current harmonics with only three active switches. These features make it attractive for electric-vehicle (EV) fast-charging stations and telecommunication power supplies, where grid-side current quality is regulated by standards such as IEEE 519 (Aretxabaleta et al., 2021; Lu et al., 2021; Shelar et al., 2024). The rectifier is normally operated with a cascaded control structure: an outer loop regulates the DC-link voltage and provides the active-current reference, inner loops regulate the line currents in the dq frame, and an additional loop balances the two DC-link capacitor voltages by injecting a zero-sequence component (Rajendran et al., 2021; Zhang et al., 2024).

The performance of this structure depends strongly on six PI gains. Analytical design based on loop bandwidth and phase margin is transparent and reproducible (Abad et al., 2020; Åström & Hägglund, 1995), but it relies on a nominal plant model and does not explicitly account for computation delay or grid impedance (Gao et al., 2022). Nonlinear alternatives such as sliding-mode control (Tian et al., 2024; Wang et al., 2022) and model predictive control (Liu et al., 2023) improve dynamic response and robustness, yet they add implementation complexity and tuning parameters of their own, which is why cascaded PI control remains the industrial default. Metaheuristic optimisers, notably the genetic algorithm (GA) (Holland, 1992; Sastry et al., 2013) and particle swarm optimisation (PSO) (Fang et al., 2023; Kennedy & Eberhart, 1995), have therefore been used to search PI gains automatically. Gladen and Staudt (2020) applied global optimisation to the controller synthesis of a Vienna rectifier, Romasevych et al. (2020) proposed a constrained PSO for PI tuning, Rajendran et al. (2022) used PSO to enhance the dynamic voltage stability of an EV battery charger, and Zhang and Yin (2021) handled conflicting objectives with NSGA-II. These studies demonstrate clear gains over manual tuning, but their cost functions are evaluated at one nominal operating point or a small set of nominal conditions.

This is a significant limitation because converter dynamics change with load level, grid strength and component tolerances. Grid impedance in particular alters the effective plant and can destabilise current control in weak grids

(Li et al., 2024; Peng et al., 2022; Xu et al., 2023), while component tolerances and ageing shift the inductance and capacitance. Gains that are optimal at the training point may therefore be poorly damped, or even unstable, elsewhere, an overfitting problem that has rarely been quantified for Vienna rectifiers. Robust worst-case formulations have been developed for predictive and low-order controllers (Costa et al., 2024; Huang et al., 2023; Sedehi et al., 2024), but, to the author's knowledge, they have not been combined with metaheuristic tuning of all three loops of the Vienna rectifier and tested on operating conditions excluded from tuning.

The objective of this paper is to obtain cascaded PI gains for a three-phase Vienna rectifier that remain acceptable over a wide range of operating and grid conditions. Three hypotheses are tested: (H1) tuning at a single scenario degrades performance away from the training point; (H2) multi-scenario min-max tuning reduces the worst-case current THD; and (H3) it improves the DC-link voltage response. The contributions are: (i) a multi-scenario min-max cost that jointly evaluates current THD, power factor, neutral-point deviation, DC-link deviation and settling time over nine training scenarios that include weak grid, unbalance and L/C mismatch; (ii) a systematic comparison of the proposed robust GA with two analytical designs, a single-scenario GA and a robust PSO, using averaged and switched models, five random seeds and three scenarios unseen during tuning; and (iii) a quantitative demonstration of single-point overfitting, supported by sensitivity and harmonic-compliance analyses. Section II describes the system model, the control structure and baseline design, and the tuning method; Section III presents and discusses the results; and Section IV concludes the paper.

II. Method

A. System Description and Modelling

1) Power stage

The converter is a three-phase Vienna rectifier (Aretxabaleta et al., 2021; Molligoda et al., 2022) with boost inductors L of series resistance R, a grid inductance L_g that represents the grid strength (nominally 0.1 mH, Table 2), and two series DC-link capacitors C_1 and C_2 feeding a resistive load R_L (98 Ω at rated power). The power stage is shown in Fig. 1 and the rated data are listed in Table 1.

Table 1. System Parameters

Parameter	Value
Grid line-to-line voltage / frequency	380 V / 50 Hz
Rated power	5 kW
DC-link voltage reference V_{dc}	700 V (350 V per capacitor)
Switching / control frequency	20 kHz (T_s = 50 µs)
Boost inductor L (resistance R)	2 mH (0.1 Ω)
DC capacitors $C_1 = C_2$	3300 µF
Simulation length / load step instant	0.4 s / 0.2 s

The DC-link voltage was chosen above twice the peak phase voltage (2 × 310 V) so that the converter operates in its linear modulation range; the resulting modulation index, defined as $2\hat{E}_{ph}/V_{dc}$, is about 0.89. The boost inductance was sized for a peak-to-peak switching ripple of about 20 % of the rated peak current (≈10.7 A), and the capacitors for a DC-link ripple of about 2 % (Guo et al., 2023).

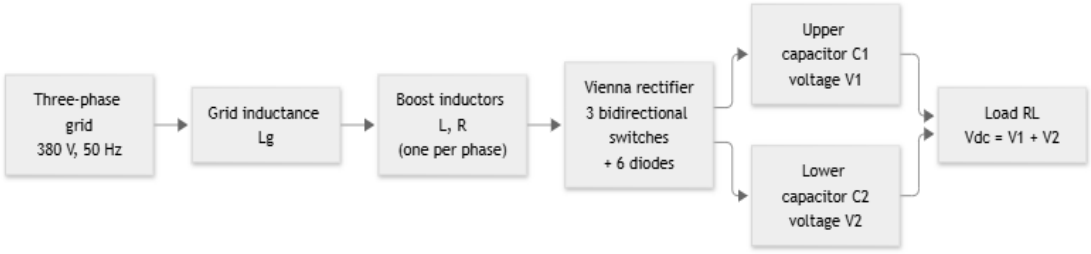


Fig. 1. Block diagram of the power stage for the studied three-phase Vienna rectifier.

2) Model equations

Let (i_k) be the phase currents (e_k) the grid voltages, and (V_1, V_2) the capacitor voltages. For each phase the fraction of the period during which the diode path conducts is m_k ($0 \le m_k \le 1$), and the pole voltage relative to the DC midpoint is

$$v_{k0} = m_k \cdot V_1, \text{ if } i_k \geq 0 \quad (1)$$

and

$$v_{k0} = -m_k \cdot V_2, \text{ if } i_k < 0 \quad (2)$$

The phase currents follow

$$(L + L_g) \cdot \frac{di_k}{dt} = e_k - R \cdot i_k - v_{k0} + \frac{1}{3} \cdot \sum_j v_{j0} \quad (3)$$

and the capacitor voltages follow

$$C_1 \cdot \frac{dV_1}{dt} = \sum_{i_k>0} m_k \cdot i_k - \frac{(V_1 + V_2)}{R_L} \quad (4)$$

$$C_2 \cdot \frac{dV_2}{dt} = -\sum_{i_k<0} m_k \cdot i_k - \frac{(V_1 + V_2)}{R_L} \quad (5)$$

In (1)–(5) the semiconductor switches are treated as ideal and dead-time is neglected. In the averaged model m_k is the duty ratio over each control period, whereas in the switched model it is realised by pulse-width modulation at 20 kHz.

B. *Control Structure and Baseline Design*

1) Cascade structure

The controller contains three loops:

(i) the dq current loops with decoupling and grid-voltage feed-forward (Abad et al., 2020; Ahmed & Çelik, 2022; Rajendran et al., 2021);
(ii) the outer DC voltage PI loop that outputs the d-axis current reference; and
(iii) a neutral point PI loop acting on $\Delta V = V_1 - V_2$ that outputs a zero sequence voltage added to the three modulation references.

One control period of computation delay is included, and the voltage reference angle is advanced by $1.5 \cdot T_s$ to compensate it (Gao et al., 2022). The structure is shown in Fig. 2.

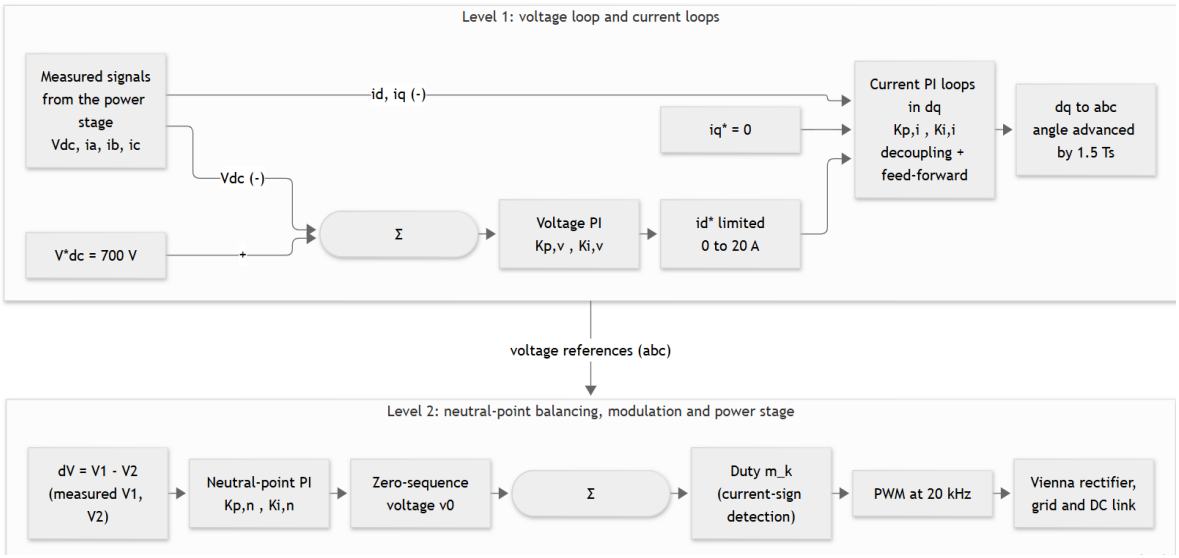


Fig. 2. Cascaded control structure: DC voltage loop, dq current loops and neutral-point balancing loop.

2) Baseline (manual) design

The two reference controllers were designed analytically. The current-loop proportional gain is $K_{p,i} = \omega_{ci} \cdot L$ with a crossover frequency of 1 kHz ($\omega_{ci} = 2\pi \cdot 1000$ rad/s), giving $K_{p,i} = 12.566$, and the integral gain places the PI zero at 100 Hz ($K_{i,i} = 2\pi \cdot 100 \cdot K_{p,i} = 7895.7$). The voltage-loop proportional gain is $K_{p,v} = \omega_{cv} \cdot C_{eq} \cdot V_{dc}/(1.5 \cdot \hat{E}_{ph})$, where $C_{eq} = C_1C_2/(C_1 + C_2) = 1650$ µF and $\hat{E}_{ph}$ is the peak phase voltage, and the PI zero is placed at one quarter of the crossover frequency ($K_{i,v} = 2\pi \cdot (f_{cv}/4) \cdot K_{p,v}$). A crossover frequency $f_{cv} = 20$ Hz gives the conventional design ($K_{p,v} = 0.3119$, $K_{i,v} = 9.797$) and $f_{cv} = 50$ Hz gives the fast design ($K_{p,v} = 0.7797$, $K_{i,v} = 61.23$). Both designs use unity neutral-point gains. All baseline gains are listed in Table 3.

C. Tuning Method

1) Decision variables and bounds

The six gains ($K_{p,i}$, $K_{i,i}$, $K_{p,v}$, $K_{i,v}$, $K_{p,n}$, $K_{i,n}$) are optimised as multipliers of the corresponding 20 Hz baseline gains (Section II.B.2). The bounds on the multipliers were 0.5–2 for $K_{p,i}$, 0.2–3 for $K_{i,i}$, 0.3–6 for $K_{p,v}$, 0.3–8 for $K_{i,v}$ and 0.2–5 for both neutral-point gains. The upper bound of $K_{p,i}$ keeps the current loop stable for an inductance down to 0.6 times nominal, and the upper bound of $K_{p,v}$ keeps the voltage-loop bandwidth below about one-eighth of the current-loop bandwidth to preserve cascade separation.

2) Operating scenarios

Twelve scenarios were defined (Table 2). Scenarios 1–9 are used for training and were chosen to cover the main sources of variation in practice: load level (scenarios 1–2), load steps in both directions (3–4), weak grid (5), voltage unbalance (6), a combined worst case (7), and reduced inductance and capacitance representing tolerances and ageing (8–9). Scenarios A–C combine these factors in ways never seen by the optimisers. Their parameters lie within the training envelope, so they test interpolation between training conditions rather than extrapolation beyond them; extrapolation is examined separately in the sensitivity analysis (Section III.E).

Table 2. Operating Scenarios

No.	Name	Load	L_g	L / C scale	Unbalance
1	Rated 100 %	5 kW	0.1 mH	1 / 1	0
2	Light 20 %	1 kW	0.1 mH	1 / 1	0
3	Step 50→100 %	2.5→5 kW	0.1 mH	1 / 1	0
4	Step 100→50 %	5→2.5 kW	0.1 mH	1 / 1	0
5	Weak grid + step	2.5→5 kW	10 mH	1 / 1	0
6	Unbalance 3 %	5 kW	0.1 mH	1 / 1	3 %
7	Harsh weak + mismatch	2→5 kW	15 mH	0.7 / 0.7	2 %
8	Low L 0.6× + step	2.5→5 kW	0.1 mH	0.6 / 1	0
9	Low L 0.8× light	1 kW	0.1 mH	0.8 / 0.7	0
A	Unseen A	1→4 kW	5 mH	0.8 / 0.7	0
B	Unseen B	4→1.5 kW	0.5 mH	1.2 / 1.3	2 %
C	Unseen C	3→5 kW	2 mH	0.7 / 1	0

D. The following metrics are calculated for each scenario:

(i) the total harmonic distortion (THD) of the phase currents, including harmonics 2 to 50, computed over one fundamental cycle and averaged over a 0.1 s window before the load change and at the end of the simulation, taking the maximum over the three phases; (ii) the power factor (PF) over the same windows, taking the worst value; (iii) the peak neutral-point deviation $\Delta V_{pk} = \max|V_1 - V_2|$; (iv) the DC-voltage deviation dev = $\max|\bar{V}_{dc} - V_{dc}|$, *where* V_{dc} is the reference and $\bar{V}_{dc}$ is the 20 ms moving average of V_{dc}, which removes ripple at multiples of 50 Hz; and (v) the settling time t_s, defined as the last instant after a load change at which the filtered deviation exceeds ±0.3 % (2.1 V). A settling time of zero therefore indicates that the deviation never left this band.

1) Cost function

For each scenario s the cost is

$$J_s = \frac{\mathrm{THD}}{5} + \frac{\Delta V_{pk}}{10} + \frac{\mathrm{dev}}{15} + \frac{t_s}{0.1} + \frac{1 - \mathrm{PF}}{0.01} \tag{6}$$

where THD is in %, voltages in V and t_s in s. Each normaliser corresponds to an acceptability threshold, so that a term equal to one marks a borderline design: 5 % THD (the IEEE 519 total demand distortion limit for low-voltage systems; Shelar et al., 2024), 10 V neutral-point deviation, 15 V DC-link deviation, 100 ms settling time and a power factor of 0.99. A penalty of $10\cdot(\mathrm{THD}/5 - 1)$ is added when THD exceeds 5 %, and $10\cdot(\Delta V_{pk}/10 - 1)$ when ΔV_{pk} exceeds 10 V; a run that diverges receives $J_s = 1000$. The robust cost over the scenario set is a worst-case (min-max) formulation in the sense of Costa et al. (2024) and Huang et al. (2023):

$$J = \max_s J_s + 0.2 \cdot \frac{1}{N} \sum_s J_s, \; N = 9 \tag{7}$$

The worst-case term drives the optimisation, while the small mean term (weight 0.2) acts as a tie-breaker that rewards designs which also perform well in the non-critical scenarios. The weights are engineering choices; a systematic study of their influence is left for future work.

2) Optimizers

The GA (Holland, 1992; Sastry et al., 2013) is real-coded with population 24, 20 generations, two elites, tournament selection (size 3), blend crossover (coefficient range 0.25 to 1.25), and Gaussian mutation (probability 0.25 per gene, standard deviation 15 % of the range). The first individual is the 20 Hz manual design. The PSO (Kennedy & Eberhart, 1995) uses the same population and number of iterations, inertia weight (Fang et al., 2023) decreasing from 0.9 to 0.4, acceleration coefficients 1.6, and a velocity limit of 20 % of the range. Both are run for five random seeds on the robust cost (nine training scenarios). A further GA is run for five seeds on scenario 3 only (Step 50→100 %) to represent single operating-point tuning. The averaged model is used inside the optimization loop, and the final gains are verified with the switching model. The procedure is summarized in Fig. 3. With these settings each run requires 480 cost evaluations (4,320 scenario simulations for the robust cost), and both optimisers use the same evaluation budget.

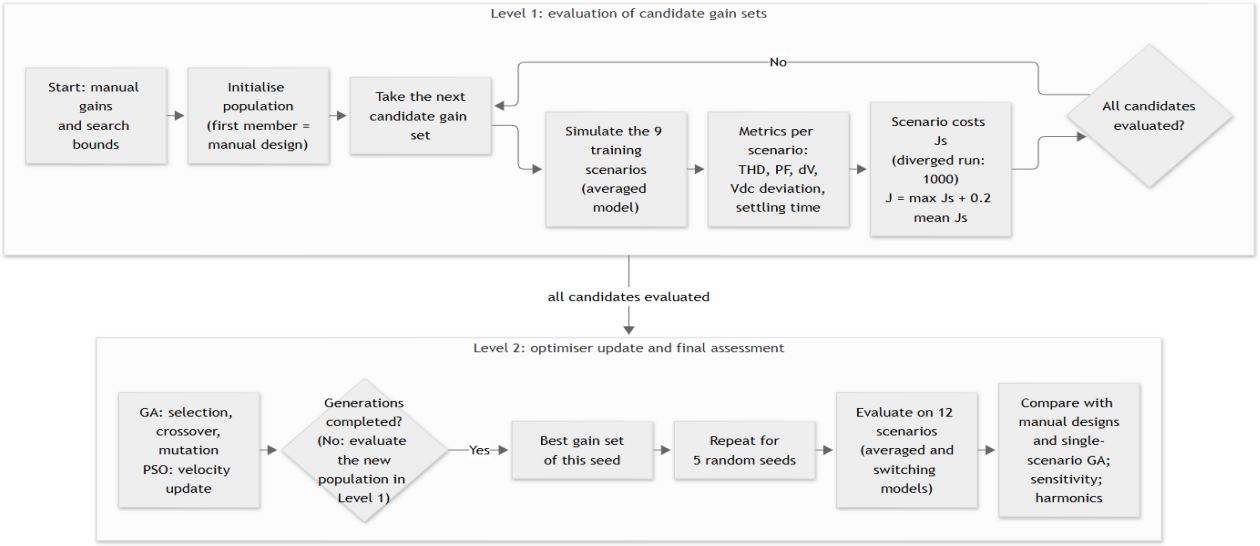


Fig. 3. Flowchart of the proposed robust multi scenario tuning procedure.

III. Results and Discussion

The gains of the best seed of each optimiser are given in Table 3.

Table 3. Controller Gains

Method	$K_{p,i}$	$K_{i,i}$	$K_{p,v}$	$K_{i,v}$	$K_{p,n}$	$K_{i,n}$
Manual 20 Hz	12.566	7895.7	0.3119	9.797	1.000	1.000
Manual 50 Hz	12.566	7895.7	0.7797	61.234	1.000	1.000
GA single-scenario	18.440	23687.1	1.8712	78.379	0.307	0.297
GA robust (proposed)	24.779	1579.1	0.4889	78.379	0.200	1.666
PSO robust	24.717	2006.1	0.4750	78.379	0.323	0.958

A. Worst Case over All Twelve Scenarios

Table 4. Worst-Case Metrics over the Twelve Scenarios (Averaged Model / Switching Model)

Method	Max THD (%)	Min PF	Max ΔV_{pk} (V)	Max V_{dc} deviation (V)	Max settling (ms)
Manual 20 Hz	4.12 / 4.12	0.9992 / 0.9992	2.66 / 2.67	14.0 / 14.0	75.9 / 76.0
Manual 50 Hz	4.46 / 4.38	0.9987 / 0.9988	3.78 / 3.76	4.3 / 4.3	21.2 / 21.2
GA single-scenario	14.52 / 21.26	0.7834 / 0.7786	8.20 / 10.51	2.3 / 2.3	181.7 / 31.3
GA robust (proposed)	2.56 / 2.56	0.9996 / 0.9996	3.07 / 3.08	4.3 / 4.3	18.3 / 18.3
PSO robust	2.59 / 2.58	0.9996 / 0.9996	3.02 / 3.03	4.3 / 4.3	18.3 / 18.4

The averaged and switching models agree closely for all methods except the single-scenario GA, whose poorly damped, oscillatory response makes the threshold-based settling time differ between the two models. The robust GA has the lowest worst-case THD, 38 % lower than the 20 Hz manual design and 43 % lower than the 50 Hz design. Its worst-case voltage deviation is 69 % lower than that of the 20 Hz design and equal to that of the 50 Hz design, and its worst-case settling time is 76 % shorter than the 20 Hz design and 14 % shorter than the 50 Hz design. The

single-scenario GA has the smallest worst-case voltage deviation (2.3 V), but also the highest THD and the lowest power factor.

B. Per-Scenario Behavior

Table 5. Current THD (%) per Scenario, Averaged Model

Scenario	Manual 20 Hz	Manual 50 Hz	GA single	GA robust	PSO robust
1 Rated 100 %	0.31	0.31	0.15	0.18	0.19
2 Light 20 %	0.72	0.72	0.71	0.59	0.58
3 Step 50→100 %	0.31	0.31	0.15	0.18	0.19
4 Step 100→50 %	0.31	0.31	0.15	0.18	0.19
5 Weak grid + step	2.36	2.38	2.44	2.05	2.15
6 Unbalance 3 %	0.72	0.95	1.38	0.80	0.81
7 Harsh weak + mismatch	4.12	4.46	14.52	2.56	2.59
8 Low L 0.6× + step	0.27	0.27	0.27	0.18	0.18
9 Low L 0.8× light	0.86	0.86	0.87	0.68	0.67
A (unseen)	1.03	1.04	0.66	0.71	0.73
B (unseen)	0.53	0.63	0.83	0.49	0.48
C (unseen)	0.58	0.58	0.46	0.39	0.40

Table 6. DC Voltage Deviation (V) / Settling Time (ms) for the Load-Step Scenarios, Averaged Model

Scenario	Manual 20 Hz	Manual 50 Hz	GA single	GA robust	PSO robust
3 Step 50→100 %	11.3 / 71.8	3.6 / 20.0	1.9 / 0	3.8 / 17.0	3.8 / 17.0
5 Weak grid + step	11.3 / 71.3	3.6 / 19.5	2.0 / 0	3.8 / 16.3	3.8 / 16.3
7 Harsh weak + mismatch	13.9 / 75.9	4.3 / 20.8	2.1 / 181.7	4.3 / 15.6	4.3 / 15.6
A (unseen)	14.0 / 75.3	4.3 / 20.8	2.3 / 13.7	4.3 / 16.4	4.3 / 16.4
B (unseen)	11.3 / 71.2	3.7 / 21.2	2.0 / 0	4.0 / 18.3	4.0 / 18.4
C (unseen)	9.0 / 66.0	2.9 / 17.2	1.6 / 0	3.0 / 15.4	3.1 / 15.5

The single-scenario GA is better than the robust controllers in the nominal step scenarios (deviation 1.9 V against 3.8 V, THD 0.15 % against 0.18 %), but in scenario 7 its THD rises to 14.52 %, the power factor falls to 0.783 and the DC-voltage ripple reaches 24 V. This ripple does not appear in Table 4 because the deviation metric is computed from the 20 ms moving average, which removes ripple at multiples of 50 Hz. This behaviour is the signature of overfitting to the training point. Over five seeds its worst-case THD is 9.89 ± 6.08 %.

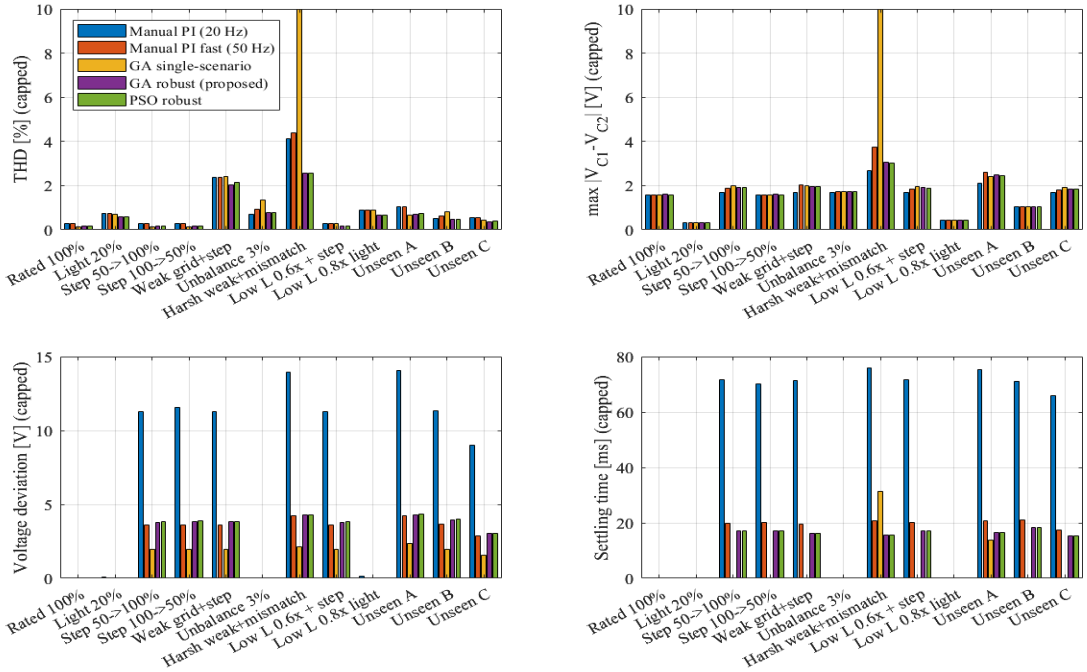


Fig. 4. Per-scenario metrics of the five controllers (THD, neutral point deviation, DC-voltage deviation and settling time). Failed or very large values are drawn at the display cap of each panel.

C. Statistics over Five Seeds

Table 7. Worst Case over Twelve Scenarios, Mean ± Standard Deviation over Five Seeds, Averaged Model

Method	Max THD (%)	Max ΔV_{pk} (V)	Max V_{dc} deviation (V)	Max settling (ms)
Manual 20 Hz (deterministic)	4.12	2.66	14.0	75.9
Manual 50 Hz (deterministic)	4.46	3.78	4.3	21.2
GA single-scenario	9.89 ± 6.08	6.99 ± 3.42	2.3 ± 0.0	47.2 ± 75.2
GA robust	2.69 ± 0.21	3.02 ± 0.11	4.3 ± 0.2	18.3 ± 0.1
PSO robust	2.67 ± 0.20	3.05 ± 0.02	4.2 ± 0.2	18.2 ± 0.1

The robust methods are consistent across seeds (THD standard deviation about 0.2 %), whereas the single-scenario GA varies strongly. The differences between the robust GA and the robust PSO lie within one standard deviation for every metric, so the two optimisers can be regarded as equivalent in this study.

D. Time Responses and Convergence

Fig. 5 shows the convergence of the best cost. All three optimisers improve rapidly during the first five generations and change little after about generation 14, indicating that the 20-generation budget is adequate for this six-variable problem. The robust GA and robust PSO converge to practically the same cost (about 1.42), whereas the single-scenario GA reaches a much lower value (about 0.43) because its cost is evaluated on a single, benign scenario. Fig. 6 compares representative time responses. For the 50→100 % load step, the 20 Hz manual design shows the deepest dip (to about 688 V) and the slowest recovery, while the robust controllers dip to about 694 V and recover within about 50 ms with a small overshoot; the single-scenario GA has the smallest dip. In the weak-grid step the single-scenario GA oscillates immediately after the step, consistent with its poor damping at high L_g. Under 3 % unbalance the neutral-point voltage difference stays within about ±1.6 V for all controllers, and the phase current at 20 % load is sinusoidal for all methods. The dips in Fig. 6 are instantaneous values, whereas Table 6 reports the 20 ms moving-average deviation.

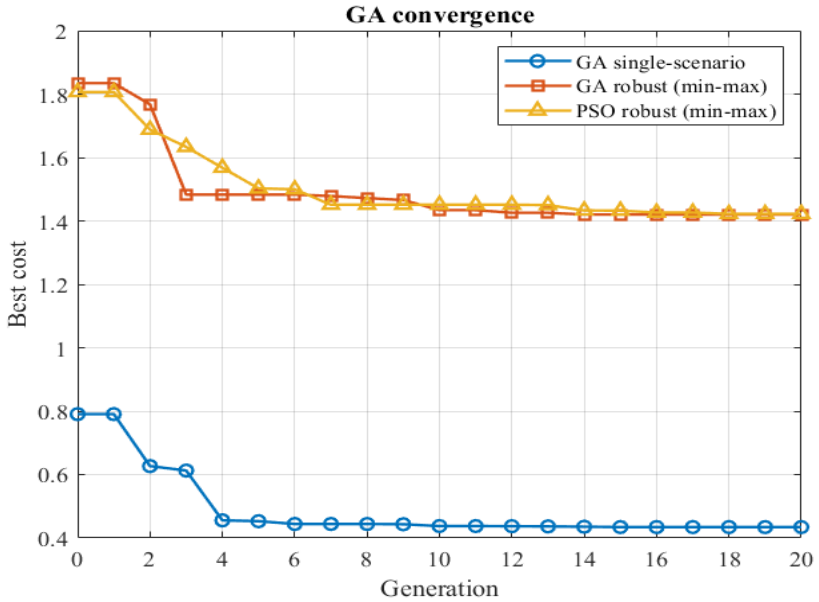


Fig. 5. Convergence of the best cost for the single-scenario GA, the robust GA and the robust PSO (best seed of each).

Frontier Energy System and Power Engineering (FESPE)
Vol. 8, Issue 1, January 2026, pp. 33-44 e-ISSN: 2654-5667

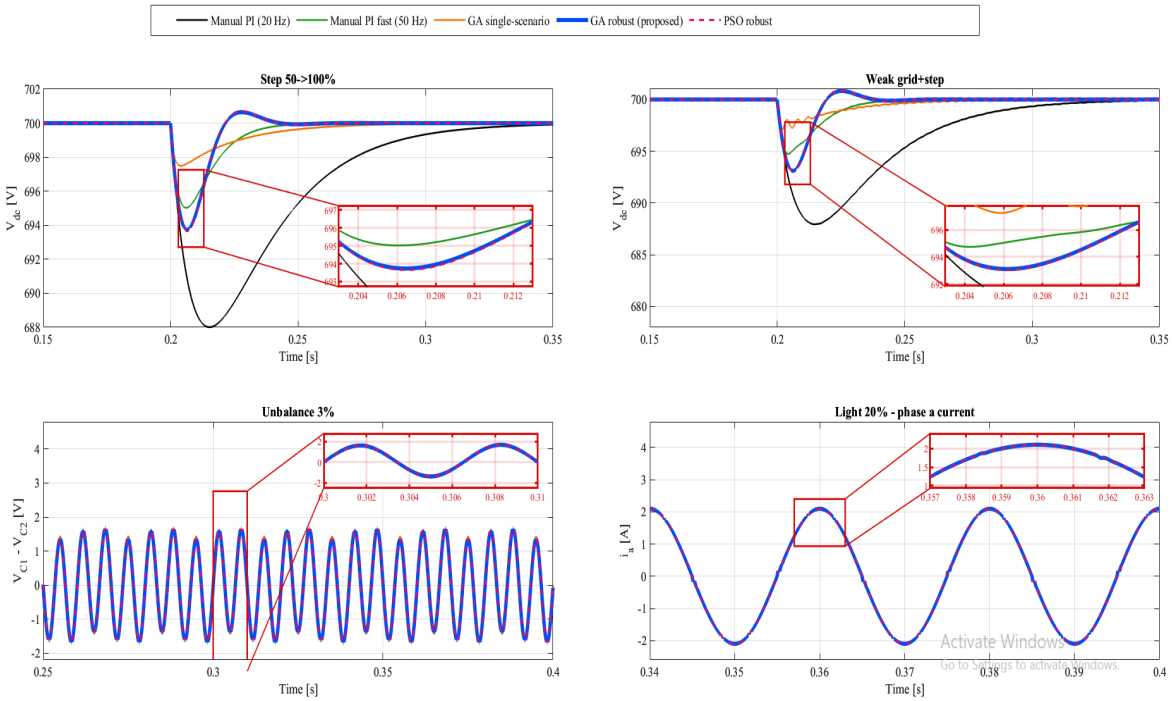


Fig. 6. Time responses: DC-link voltage for the 50 to 100 % load step and for the weak grid step, neutral-point voltage difference under 3 % unbalance, and phase a current at 20 % load.

E. Sensitivity Analysis

The inductance (0.6 to 1.4 times nominal), the capacitance (0.6 to 1.4 times) and the grid inductance (0.1 to 20 mH) were varied one at a time around the 50→100 % step scenario; the results are shown in Fig. 7. The voltage deviation of every method is almost independent of L and L_g. The current THD increases with L_g for all methods: at L_g = 20 mH it is about 3.8 % for the robust controllers, about 4 % for the manual designs and above 10 % for the single-scenario GA, which already exceeds 6 % at 15 mH. Because 20 mH lies outside the training range ($L_g \leq 15$ mH), this point also indicates that the robust gains extrapolate reasonably. No method became unstable over the tested range of L; including the low-inductance training scenarios (8 and 9) in the robust cost was necessary to obtain this property.

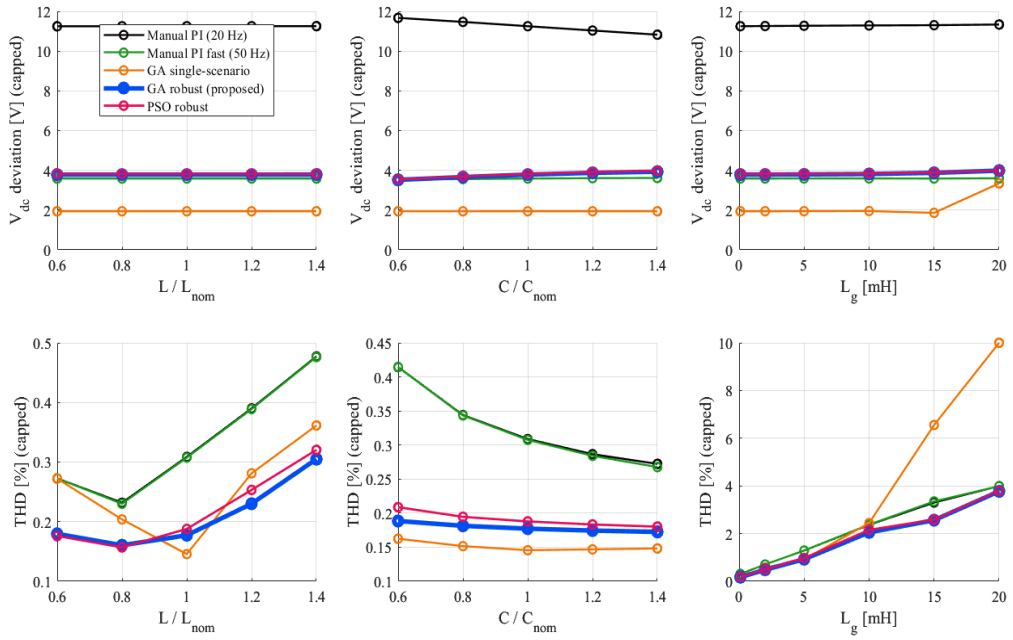


Fig. 7. Sensitivity of the DC voltage deviation (top) and of the current THD (bottom) to the inductance L, the capacitance C and the grid inductance L_g. Values above the display cap are clipped.

F. Harmonic Compliance

Fig. 8 shows the phase-a current spectrum in the weak-grid scenario, where the 5th and 7th harmonics dominate. The largest individual harmonic is 1.38 % (manual 20 Hz), 1.41 % (manual 50 Hz), 1.86 % (single-scenario GA), 1.01 % (robust GA) and 1.04 % (robust PSO). Relative to the IEEE 519 individual-harmonic limits (Shelar et al., 2024), the largest harmonic-to-limit ratio is 0.34, 0.35, 0.46, 0.37 and 0.38, respectively, so all controllers comply in this scenario. For the robust controllers the ratio of the dominant 5th harmonic is only about 0.25; their highest ratio is set by a higher-order component, for which the limit is stricter, which explains why it slightly exceeds that of the manual designs despite their lower dominant harmonics.

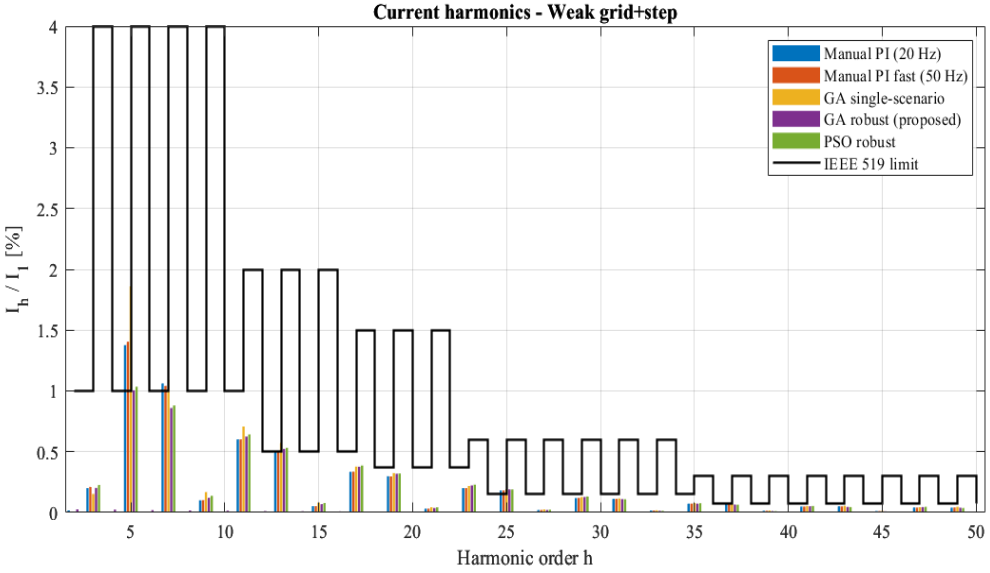


Fig. 8. Current harmonic spectrum (phase a) in the weak grid scenario.

G. Discussion

The results support the three hypotheses stated in Section I.

H1 – Single-scenario tuning overfits. The single-scenario GA gives the best nominal step response, but in the harsh weak-grid scenario its THD rises to 14.5 % (21.3 % in the switched model) and its power factor drops to 0.78; over five seeds its worst-case THD is 9.89 ± 6.08 %. A plausible explanation is that the high $K_{i,i}$ and $K_{p,v}$ obtained at the stiff-grid training point leave little damping margin once L_g increases, which is consistent with the known destabilising effect of grid impedance on current control (Li et al., 2024; Peng et al., 2022). This confirms, for the Vienna rectifier, that optimisation at a nominal operating point (Gladen & Staudt, 2020; Romasevych et al., 2020) cannot guarantee performance elsewhere, and shows that the risk is not merely a slight loss of optimality but a possible violation of power-quality limits.

H2 – Robust tuning reduces the worst-case THD. The robust GA lowers the worst-case THD to 2.56 % with a seed-to-seed standard deviation of only about 0.2 %. The improvement is concentrated in the weak-grid scenarios (5 and 7), whereas all methods keep the THD below 1 % under nominal conditions. The robust gains combine a higher current-loop proportional gain with a much lower current-loop integral gain than the manual design (Table 3); the optimiser thus trades low-frequency tracking for damping, which appears to be the key to tolerating a weak grid. Comparable conclusions, namely that robustness to filter and grid parameter uncertainty must be designed in explicitly, have been reported for predictive current control (Costa et al., 2024) and for sliding-mode control of Vienna rectifiers under unbalanced weak grids (Tian et al., 2024). The present results show that a similar benefit can be obtained with the standard cascaded PI structure, without changing the control law.

H3 – Robust tuning improves the DC-voltage response. Relative to the conventional 20 Hz design, the worst-case DC deviation is reduced by 69 % and the settling time by 76 %. Relative to the faster 50 Hz manual design, however, the deviation is identical and the settling time is only 14 % shorter. Most of the dynamic improvement over the conventional design is therefore attributable to a faster voltage loop, which a designer could also select manually. The distinctive value of the proposed method is that it delivers this speed together with the lowest worst-case THD and without overfitting. The price, compared with the single-scenario GA, is a larger deviation in the nominal step response (3.8 V versus 1.9 V), which is the cost of robustness.

Choice of optimiser. Within the robust framework, the GA and PSO reach nearly identical performance and cost. Together with the fact that $K_{i,v}$ reached its upper bound for all optimisers, this suggests that the robustness is provided by the min-max formulation rather than by the search algorithm, and that widening the $K_{i,v}$ bound may improve the results further. Compared with multi-objective approaches such as NSGA-II (Zhang & Yin, 2021), the scalarised min-max cost yields a single design directly, at the price of weights that must be chosen by the designer.

Limitations. The study is simulation-based. The plant model uses ideal switches without dead-time, and the averaged model is used inside the optimisation loop; although the final gains were verified with the switched model, losses, measurement noise and grid-voltage harmonics were not modelled. The unseen scenarios lie within the training envelope, and the cost-function weights were not varied systematically.

IV. Conclusion

This paper proposed a multi-scenario min-max tuning procedure for the cascaded PI controllers of a three-phase Vienna rectifier and compared it with two analytical designs, a single-scenario GA and a robust PSO over twelve scenarios (three unseen during tuning) and five random seeds. Tuning at a single operating point produced an excellent controller near that point but failed in the worst case, with a THD of up to 21.3 % and a power factor of 0.78. The robust min-max formulation avoided this failure, achieving a worst-case THD of 2.56 % (versus 4.12 % and 4.46 % for the manual designs), a power factor of at least 0.9996, a worst-case DC-link deviation of 4.3 V and a worst-case settling time of 18.3 ms. The GA and PSO gave practically the same results, indicating that the benefit stems from the formulation rather than from the optimiser. For practitioners, the results show that the scenario set used during tuning matters more than the choice of metaheuristic: including weak-grid and low-inductance cases in the cost is sufficient to obtain PI gains that remain compliant with harmonic limits across realistic grid and component variations, without changing the control structure or the controller hardware. The conclusions are limited to simulation with idealised switching models and to operating conditions largely within the training envelope. Future work will validate the gains through circuit-level and hardware-in-the-loop simulation and on a laboratory prototype, extend the search bounds and the scenario set (including grid-voltage harmonics and conditions outside the training range), study the sensitivity to the cost-function weights, and compare the approach with model predictive (Liu et al., 2023) and sliding-mode controllers (Tian et al., 2024).

Author Contributions

Mohammed Obayes Yousif: Conceptualization, Methodology, Software, Formal analysis, Investigation, Validation, Visualization, Writing – original draft, Writing – review & editing.

The author has read and approved the final manuscript.

Funding

No funding support was received.

Declaration of Conflicting Interests

The author declares no potential conflicts of interest with respect to the research, authorship, and/or publication of this article.

Ethics and Consent Declarations

Not applicable. This simulation-based study did not involve human participants, animals, or personal data; therefore, ethical approval and informed consent were not required.

Data Availability

The datasets generated during and/or analyzed during the current study are available from the corresponding author on reasonable request.

Declaration on AI Use

.

AI was used only to improve readability and language under strict human oversight; AI did not generate any content, ideas, analyses, or conclusions

.

References

Abad, G., Sanchez-Ruiz, A., Valera-García, J. J., & Milikua, A. (2020). Analysis and design guidelines for current control loops of grid-connected converters based on mathematical models. *Energies*, *13*(21), Article 5849. https://doi.org/10.3390/en13215849

Ahmed, H., & Çelik, D. (2022). Sliding mode based adaptive linear neuron proportional resonant control of Vienna rectifier for performance improvement of electric vehicle charging system. *Journal of Power Sources*, *542*, Article 231788. https://doi.org/10.1016/j.jpowsour.2022.231788

Aretxabaleta, I., De Alegria, I. M., Andreu, J., Kortabarria, I., & Robles, E. (2021). High-voltage stations for electric vehicle fast-charging: Trends, standards, charging modes and comparison of unity power-factor rectifiers. *IEEE Access*, *9*, 102177–102194. https://doi.org/10.1109/ACCESS.2021.3093696

Åström, K. J., & Hägglund, T. (1995). *PID controllers: Theory, design, and tuning* (2nd ed.). Instrument Society of America.

Costa, J. S., Lunardi, A., Fernandes, D. A., & Sguarezi Filho, A. J. (2024). Robust model predictive control of a renewable energy converter under parametric uncertainty conditions. *IEEE Open Journal of Power Electronics*, *5*, 123–134. https://doi.org/10.1109/OJPEL.2023.3339014

Fang, J., Liu, W., Chen, L., Lauria, S., Miron, A., & Liu, X. (2023). A survey of algorithms, applications and trends for particle swarm optimization. *International Journal of Network Dynamics and Intelligence*, *2*(1), 24–50. https://doi.org/10.53941/ijndi0201002

Gao, X., Zhou, D., Anvari-Moghaddam, A., & Blaabjerg, F. (2022). Impact of digital control delay on stability of grid-following converters. In *2022 IEEE 13th International Symposium on Power Electronics for Distributed Generation Systems (PEDG)* (pp. 1–6). IEEE. https://doi.org/10.1109/PEDG54999.2022.9923157

Gladen, M., & Staudt, V. (2020). Global optimization approach for the parameter synthesis of a pole restraining controller on the example Vienna rectifier. In *PCIM Europe digital days 2020: International Exhibition and Conference for Power Electronics, Intelligent Motion, Renewable Energy and Energy Management* (pp. 1–8). VDE.

Guo, C., Xin, Z., Han, J., Hu, L., & Lu, B. (2023). Review of the calculation of DC-link capacitor current. *Frontiers in Energy Research*, *11*, Article 1240755. https://doi.org/10.3389/fenrg.2023.1240755

Holland, J. H. (1992). *Adaptation in natural and artificial systems: An introductory analysis with applications to biology, control, and artificial intelligence*. MIT Press.

Huang, L., Zhen, J., Lygeros, J., & Dörfler, F. (2023). Robust data-enabled predictive control: Tractable formulations and performance guarantees. *IEEE Transactions on Automatic Control*, *68*(5), 3163–3170. https://doi.org/10.1109/TAC.2023.3241282

Kennedy, J., & Eberhart, R. (1995). Particle swarm optimization. In *Proceedings of ICNN'95 – International Conference on Neural Networks* (Vol. 4, pp. 1942–1948). IEEE. https://doi.org/10.1109/ICNN.1995.488968

Li, M., Zhang, X., Fu, X., Geng, H., & Zhao, W. (2024). Stability studies on PV grid-connected inverters under weak grid: A review. *Chinese Journal of Electrical Engineering*, *10*(4), 1–19. https://doi.org/10.23919/CJEE.2024.000081

Liu, C., Xing, X., Du, C., Zhang, B., Zhang, C., & Blaabjerg, F. (2023). An improved model predictive control method using optimized voltage vectors for Vienna rectifier with fixed switching frequency. *IEEE Transactions on Power Electronics*, *38*(1), 358–371. https://doi.org/10.1109/TPEL.2022.3205946

Lu, Y., Liu, Z., Meng, S., Ji, J., & Lyu, J. (2021). Deadbeat predictive power control for Vienna rectifier under unbalanced power grid condition. *Energy Reports*, *7*, 257–266. https://doi.org/10.1016/j.egyr.2021.08.048

Molligoda, D., Ceballos, S., Pou, J., Satpathi, K., Sasongko, F., Gajanayake, C., & Gupta, A. (2022). Hybrid modulation strategy for the Vienna rectifier. *IEEE Transactions on Power Electronics*, *37*(2), 1283–1295. https://doi.org/10.1109/TPEL.2021.3103766

Peng, Q., Buticchi, G., Tan, N. M. L., Guenter, S., Yang, J., & Wheeler, P. (2022). Modeling techniques and stability analysis tools for grid-connected converters. *IEEE Open Journal of Power Electronics*, *3*, 450–467. https://doi.org/10.1109/OJPEL.2022.3190103

Rajendran, G., Vaithilingam, C. A., Misron, N., Naidu, K., & Ahmed, M. R. (2021). Voltage oriented controller based Vienna rectifier for electric vehicle charging stations. *IEEE Access*, *9*, 50798–50809. https://doi.org/10.1109/ACCESS.2021.3068653

Rajendran, G., Vaithilingam, C. A., Naidu, K., Alsakati, A. A., Oruganti, K. S. P., & Fauzan, M. F. (2022). Dynamic voltage stability enhancement in electric vehicle battery charger using particle swarm optimization. *IEEE Access*, *10*, 97767–97779. https://doi.org/10.1109/ACCESS.2022.3199416

Romasevych, Y., Loveikin, V., & Makarets, V. (2020). Optimal constrained tuning of PI-controllers via a new PSO-based technique. *International Journal of Swarm Intelligence Research*, *11*(4), 87–105. https://doi.org/10.4018/IJSIR.2020100104

Sastry, K., Goldberg, D. E., & Kendall, G. (2013). Genetic algorithms. In E. K. Burke & G. Kendall (Eds.), *Search methodologies: Introductory tutorials in optimization and decision support techniques* (2nd ed., pp. 93–117). Springer. https://doi.org/10.1007/978-1-4614-6940-7_4

Sedehi, A., Alfi, A., & Mirjafari, M. (2024). Low-order robust controller for DC-DC quadratic buck converter: Design and implementation. *Journal of AI and Data Mining*, *12*(1), 15–25. https://doi.org/10.22044/jadm.2024.13584.2475

Shelar, S., Bankar, D., & Bakre, S. (2024). Review of revisions of IEEE 519 standard on power system harmonics (1981 to 2022). In *2024 21st International Conference on Harmonics and Quality of Power (ICHQP)* (pp. 415–420). IEEE. https://doi.org/10.1109/ICHQP61174.2024.10768696

Tian, Y., Yuan, H., Zhu, W., Li, X., & Li, Y. (2024). Sliding mode control of Vienna rectifier under unbalanced weak power grid. *IEEE Access*, *12*, 39095–39109. https://doi.org/10.1109/ACCESS.2024.3373701

Wang, Y., Li, Y., & Huang, S. (2022). An improved sliding mode direct power control strategy based on reactive power compensation for Vienna rectifier. *IEEE Access*, *10*, 15469–15477. https://doi.org/10.1109/ACCESS.2022.3149042

Xu, Z., Qin, Y., Li, Z., Jiao, C., Zhai, B., & Chang, X. (2023). Stability analysis of different control modes of grid-connected converters under different grid conditions. *Frontiers in Energy Research*, *11*, Article 1242024. https://doi.org/10.3389/fenrg.2023.1242024

Zhang, P., Wu, X., Li, B., Ding, L., Long, J., Zhang, W., & Li, Y. (2024). Reduction of common-mode voltage and NP voltage oscillation for three-level Vienna rectifiers using alternative phase opposition disposition PWM. *IEEE Transactions on Industrial Electronics*, *71*(8), 8237–8247. https://doi.org/10.1109/TIE.2023.3317836

Zhang, T., & Yin, X. (2021). Multi-objective PI controller tuning using NSGA-II with preferability. In *2021 40th Chinese Control Conference (CCC)* (pp. 1562–1568). IEEE. https://doi.org/10.23919/CCC52363.2021.9550634